文章编号：1001-9014(2020)03-0300-06

DOI:10.11972/j.issn.1001-9014.2020.03.006

A fast imaging algorithm for sparse array imaging based on PCA and modified SLIM methods

MENG Xiang-Xin, WU Shuai*, TU Hao, LIU Tao-Rong, JIN Xue-Ming

(Brainware Terahertz Information Technology Co. Ltd, Hefei 230000, China)

Abstract: An algorithm combining frequency domain imaging algorithm and compressed sensing (CS) framework is proposed in here for millimeter-wave multi-static sparse array imaging. The algorithm consists of two major steps. Firstly, the typical fast Fourier transform (FFT) algorithm used in square boundary array with phase center approximation (PCA) is carried out. However, the residual phase error introduced by the PCA at close range cannot be compensated completely, so in the second step, the modified sparse learning via iterative minimization (SLIM) algorithm which is in the CS framework is introduced to refocus the initial images. By combining PCA and the modified SLIM algorithm, the proposed algorithm reaches a better computational efficiency, improves the image quality, and alleviates the requirement for iterations of the original SLIM algorithm. Simulation results verify the effectiveness of this algorithm.

Key words: sparse array imaging, fft imaging algorithm, the modified SLIM algorithm, compressed sensing

PACS: 42.30.Wb

基于等效相位中心近似与改进SLIM算法的稀疏阵列快速成像算法

孟祥新, 武 帅*, 涂 昊, 柳桃荣, 靳学明

(博微太赫兹信息科技有限公司,安徽 合肥 230000)

摘要:提出一种应用于毫米波稀疏阵列成像的基于频率域成像算法和压缩感知技术相结合的成像算法。算法包含两个主要步骤,首先采用等效相位中心近似原理,将快速傅里叶变换成像算法用于周边形阵列,由于等效相位中心近似引入的残余相位误差无法在近距离成像应用中被完全补偿,因此在第二个步骤中,提出基于压缩感知技术的基于迭代最小化的稀疏学习(SLIM)的改进算法用于重聚焦初始图像。通过等效相位中心近似原理和改进的SLIM算法的结合,所提算法具备更高的计算效率、提升了图像质量、相比于传统的SLIM算法具备更少的迭代次数。仿真结果验证了所提算法的有效性。

关 键 词:稀疏阵列成像;傅里叶变换成像算法;改进的SLIM算法;压缩感知

中图分类号:O45 **文献标识码**:A

Introduction

Millimeter-wave imaging technology is widely used in earth observation [1], non-destructive testing [2], security inspection imaging [3-4], which has great commercial and scientific values. A variety of imaging configurations is able to form three-dimensional holographic images of the targeted area, such as one-dimensional array combined with mechanical scanning imaging [3-4], two-dimensional full and sparse array imaging[5-8] and single pixel real aperture imaging [9]. Two-dimensional sparse planar array technology has the advantages of fewer antennas and no mechanical scanning parts, thus it has become a research hotpot in the field of millimeter-wave three-dimensional imaging.

There have been plenty of studies concerningthe imaging algorithms for 2D sparse arrays, among which William F. Moulder preprocessed the raw back scatter data by phase center approximation (PCA) method in sparse square boundary array (BA) configuration [7-8]. The fast Fourier transform (FFT) algorithm was applied in the configuration which has improved the image reconstruc-

Received date: 2019-10-18, **revised date**: 2019-11-18 **收稿日期**:2019-10-18,**修回日期**:2019-11-18

Foundation items: Supported by Key research and development projects in Anhui Province(201904e01020005)

Biography: MENG Xiang-Xin (1990—), male(Mongolian), Chifeng, Inner Mongolia, China, Master, Research fields include millimeter wave Signal Processing and Image Reconstruction. E-mail: 15856969462@163.com

* **Corresponding author**: E-mail: shuaiwu52@163.com

tion efficiency greatly to reach a video frame rate of 10 Hz[10]. The compensation process for the PCA was performed by assuming a constant imaging distance, whereas refocusing phenomenon was obvious at close range. The larger the spacing between transmitting antennas and receiving antennas, the more difficult it was to correct the residual phase errors introduced by PCA except at the long distances. Thus, this method cannot obtain good image quality for target area at close range, while it can only work at far range where the resolution is worse for fixed aperture size.

Aiming at solving the previous issue, an improved method combining PCA and compressed sensing (CS) is proposed in this paper for the BA configuration[7-8]. A modified sparse learning via iterative minimization (SLIM) algorithm based on CS theory is utilized for refocusing at close-range, solving the problem that the FFT algorithm cannot image close-range targets accurately. The effectiveness of the proposed method is verified by simulation results.

1 Sparse array design and algorithm

1.1 The Sparse array and PCA process

The geometrical configuration of the BA used in this paper is shown in Fig. 1 with the parameters shown in Table 1. The spacing of antenna elements is set as 0.01 m which is smaller than the central wavelength $\lambda_c = 0.0111m$, resulting in a spacing of the equivalent elements of 0.005 m smaller which satisfies the criterion of less than half the central wavelength. Such a configuration ensures that no grating lobes appear in the imaging field of view.

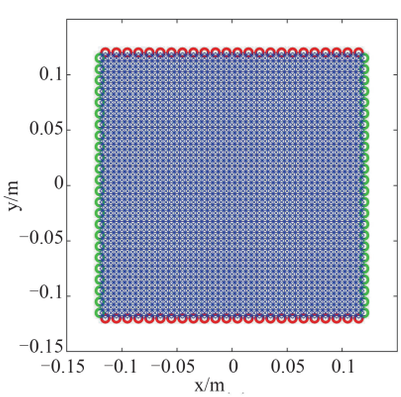

Fig. 1 The square boundary array, where the red circles represent the spatial position of the transmitting antenna and the green circles represent the spatial position of the receiving antenna, blue stars show the positions of the equivalent phase center
图1 周边型阵列,红色圆圈表示发射阵元的位置,绿色圆圈表示接收阵元的位置,蓝色星号表示等效相位中心位置

The phase center approximation process for a pair of transmitting and receiving antennas is shown in Fig. 2. The spatial coordinates(x_t, y_t, z_0) and (x_r, y_r, z_0) denotes the positions of the transmitting antenna and the receiving antenna respectively, (x_c, y_c, z_0) represents the equivalent phase center position. $P(x, y, z)$ denotes a scattering center on the target. The slant ranges between the antennas to the target point are,

$$R_t = \sqrt{(x_t - x)^2 + (y_t - y)^2 + (z_0 - z)^2} \quad ,(1)$$

$$R_r = \sqrt{(x_r - x)^2 + (y_r - y)^2 + (z_0 - z)^2} \quad .(2)$$

Then, the back-scattered signal can be express-ed as,

$$s(x_t,y_t,x_r,y_r,z) = \iiint \sigma(x,y,z)e^{-jk(R_t + R_r)}dxdydz \quad ,(3)$$

where $k = 2\pi f/c$ denotes wavenumber of the transmitted signal. After the PCA process, the back-scattered signal can be expressed as,

$$s(x_c,y_c,z_0) = \iiint \sigma(x,y,z)e^{-j2kR_c}dxdydz \quad ,(4)$$

where the slant range between the phase center position and the target point is given by,

$$R_c = \sqrt{(x_c - x)^2 + (y_c - y)^2 + (z_0 - z)^2} \quad .(5)$$

The slant range error ΔR introduced by the PCA is,

$$\Delta R = R_t + R_r - 2R_c \quad (6)$$

Therefore, the phase errors introduced by the slant range error need to be compensated as follows,

$$s_{PhaseError} = \exp(jk\Delta R) \quad (7)$$

$$s'(x_c,y_c,z_0) = s(x_c,y_c,z_0) \cdot s_{PhaseError} \quad (8)$$

where $S_{PhaseError}$ denotes the compensation factor, $s'(x_c, y_c, z_0)$ denotes the compensated signal.

By applying Eq. (8), the phase errors introduced by the PCA are compensated. But the compensation factor is only accurate for a fixed reference point on the target, where usually the center point $P_0(0, 0, z_0)$ of the target is chosen. The result of this drawback is that the phase errors cannot be compensated accurately at arbitrary positions in the target area. Also, the approximation requires the distance between the transmitting antenna and the receiving antenna to be much smaller than the target distance, in which case, the residual phase errors can be negligible. These errors can be corrected by using the modified SLIM algorithm introduced in Sect. Ⅱ. C.

1.2 FFT Algorithm

$$\sigma(\mathrm{x,y,z}) = \sum_{p}^{Nf} S(\mathrm{k}_x,\mathrm{k}_y,\mathrm{k})\mathrm{e}^{\mathrm{j}z\sqrt{4k^2 - k_x^2 - k_y^2}}\Delta k_p \quad ,(9)$$

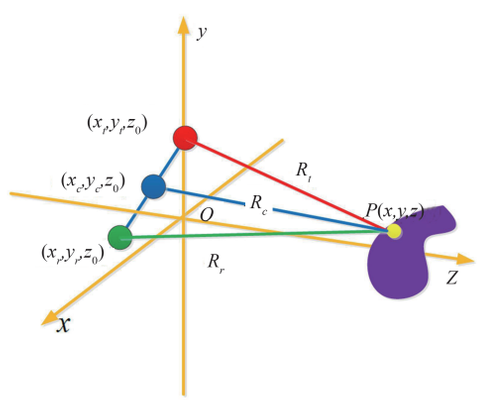

Fig. 2 Sparse array equivalent phase center schematic
图2 稀疏阵列等效相位中心示意图

Table 1 System Parameters
表1 系统参数

Parameters	Values
Frequency	24~30GHz
Sweep points	24
Unambiguous distance	0.6m
Number of transmit elements	48
Number of receive elements	48
Element spacing	0.01m

$$S(k_x,k_y,k) = FT_{2D}[s'(x_c,y_c,z_0)] \quad . \quad (10)$$

The FFT algorithm can obtain images at different ranges z_i by parallel computing, where $z_i \in [Z_{\min}, Z_{\max}]$ (for $i = 1, ..., N$), $Z_{\min}$ and $Z_{\max}$represent the minimum and maximum range in the imaging scene, N represents the number of the range position slices. The images in the different range position slices can be reconstructed parallel, thus the algorithm has high computational efficiency.

1.3 The Modified SLIM Algorithm

The imaged targets can be decomposed into a set of scattering points, which occupy only a part of the whole scene, so the targets in millimeter-wave images can be expressed sparsely. The sparse learning via iterative minimization (SLIM) algorithm is a sparse signal reconstruction algorithm based on statistical optimization[11]. In this paper, we introduce the SLIM algorithm to refocus the images obtained from the FFT algorithm.

The sparse signal model is expressed as,

$$y = Ax + n \quad , \quad (11)$$

where $y \in \Omega^{MNP \times 1}$denotes the sampled measurement vector and$A \in \Omega^{MNP \times M'N'}$denotes the transformation matrix. M denotes the number of transmit elements, N denotes the number of receive elements and P denotes the number of sweep frequencies. The volume of the back-scattered signal is$M \times N \times P$, which can be transformed to $y$with the dimension of $MNP \times 1$. M' denotes the number of the rows in the image and N' denotes the number of the columns in the image. $x \in \Omega^{M'N' \times 1}$ denotes the sparse signal to be reconstructed. $n \in \Omega^{MNP \times 1}$ denotes the additive white Gaussian noise. The original back-scattered signal, rewritten into a vector, is set as y, the transformation matrix A can be deduced from the theoretical model of the back-scattered signal,

$$A(x_t,y_t,x_r,y_r ; x,y,z) = e^{-jk(R_t + R_r)} \quad . \quad (12)$$

And the initial guess x^0 required by the SLIM algorithm is chosen as the output image from the FFT algorithm. Then the final images can be numerically solved by the SLIM algorithm, the details of the SLIM algorithm can be found in Ref. [11].

The imaged targets in the image are sparse in the whole image because the effective pixels account for a small part of all pixels and the rest are background. It is not necessary to input all the pixels of the distorted images to the SLIM algorithm, so the effective pixels of the target in the images can be selected in advance and the transformation matrix A is not necessary to input into the algorithm wholly. The number of effective pixels is smaller than the total pixels, and then it can be utilized to reduce the computational complexity of the SLIM algorithm. The method of selecting effective pixels can be converting the initial distorted images to logarithmic images, and setting a logarithmic threshold to select the pixels and the effective positions.

From this point of view that decreasing the input data volume to improve the SLIM algorithm, a modified SLIM algorithm is described below,

(1) Converting the distorted image I to a normalized logarithmic-scale imageI_dB.

(2) Setting a logarithmic threshold Th_dB to obtain the voxels where $Posi\_Th = Posi[I\_dB > Th\_dB]$.

(3) Setting $A\_Th = A[Posi\_Th]$ as the new transformation matrix and $x\_Th = I[Posi\_Th]$ as the initial sparse signal vector.

(4) The matrixA_Th and the vector $x_Th$are set as initial input data of the typical SLIM algorithm to solve the sparse signalx_newTh.

(5) Then the final reconstructed signal x can be expressed as$x[Posi_Th] = x_newTh$.

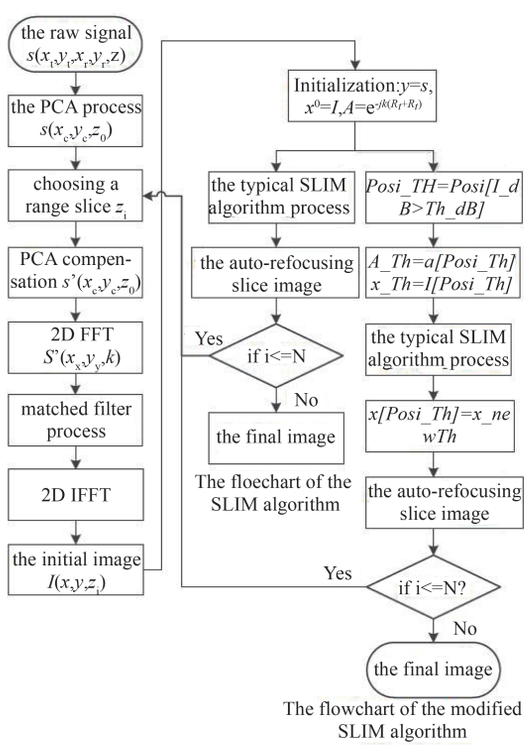

Fig. 3 The main steps of the proposed algorithm
图3 所提算法主要步骤

It can be seen that the modified SLIM algorithm can improve the computational efficiency by reducing the data volume of the transformation matrix A and the sparse signal x. Only the targets in the distorted images need to be reconstructed while other weak voxels are discarded. In this process, auto-focusing accuracy is also improved by the modified SLIM algorithm. The precondition of the

modified SLIM algorithm is that the targets are sparse in the scenario, such as through-the-wall radar imaging, ground penetrating imaging and nondestructive testing imaging. If the targets' sparse character is not obvious; the improvement of calculation efficiency is also not significant. Then the main steps of the proposed algorithm are shown in Fig. 3.

2 Experimental Results and Discussion

2.1 Points targets simulation

To verify the effectiveness of the proposed method, the back-scattered signal of nine point targets is simulated by MATLAB using the geometrical optics method (GO). The central range between the targets and the plane of BA is set at 0.2 m. The algorithms have been implemented by MATLAB codes based on a multi-core workstation equipped with a Xeon W-2195 CPU @ 2.30 GHz and 64.0 GB RAM.

The reconstruction results are shown in Fig. 4 and the red circles represent the real positions of the nine point target. It can be seen that the image of the FFT algorithm based on PCA is distorted because the maximum distance between the transmitting antennas and the receiving antennas is larger than 0.2 m, thus the residual phase error cannot be neglected in this condition. As shown in Fig. 4 (b) and (c), the focusing quality of the auto-focus images is obviously improved compared to that of the FFT algorithm. At the same time, the computation time of the modified SLIM algorithm is shorter than that of the typical SLIM algorithm as shown in Table 2.

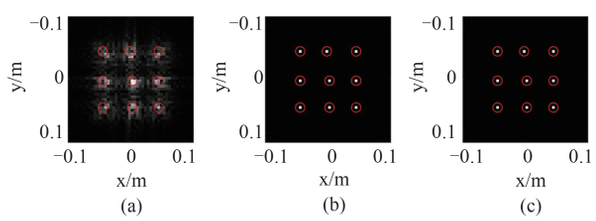

Fig. 4 (a) The original image generated by the FFT algorithm (b) The auto- focus image generated by the SLIM algorithm (iteration number = 2) (c) The auto-focus image generated by the modified SLIM algorithm (Th_dB = -15dB and no iteration)
图4 (a)FFT算法初始图像(b)SLIM算法自聚焦图像(c)改进SLIM算法自聚焦图像

Table 2 Computing time
表2 计算时间

algorithm	SLIM algorithm	Modified SLIM algorithm
Time/s	19.18	3.82

2.2 Simulation of Complex Targets

The electromagnetic simulation software is used to simulate the back-scattered signal of the complex targets comprised of letters made from metal strips. The target is shown in Fig. 5 and the final images are shown in Fig. 6. The image of the FFT algorithm is distorted in Fig. 6 (a) because the phase errors introduced by the PCA cannot be corrected completely. The focusing quality of the auto-focus images shown in Fig. 6 (b) and (c) is better than that of the FFT algorithm. The computation time of the modified SLIM algorithm is approximately a quarter of the typical SLIM algorithm, as shown in Table 3, which improves efficiency to a large extent.

Fig. 5 The simulation model of THZ letter.
图5 THZ字母的仿真模型

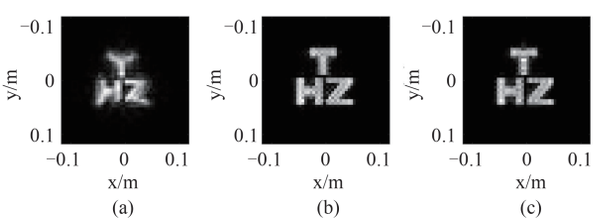

Fig. 6 (a) The original image generated by the FFT algorithm (b) The auto-focus image generated by the SLIM algorithm (iteration number = 2) (c) The auto-focus image generated by the modified SLIM algorithm (Th_dB = -20dB and no iteration)
图6 (a)FFT算法初始图像(b)SLIM算法自聚焦图像(迭代次数2)(c)改进SLIM算法自聚焦图像(Th_dB = -20dB,无迭代)

Table 3 Computing time
表3 计算时间

algorithm	SLIM algorithm	Modified SLIM algorithm
Time/s	20.63	2.45

2.3 Simulation under Noisy Environment

Random noise whose relative magnitude is between -40dB~0dB is added into the back-scattered data of the complex target to test the robustness to noise of different algorithms. The image contrast criterion used in Ref. [12] is introduced to evaluate the quality of the images. The larger value of the image contrast is, the better quality of the image is. The comparisons of image contrast are listed in Table 4.

It can be seen that image contrast of the two auto-focus algorithms is larger than those of the FFT algorithm for all different noise levels. In the meanwhile, the image contrast of the modified SLIM algorithm is better than that of the typical SLIM algorithm. The simulation results verify the ability to suppress noise of the two auto-focus algorithms, and the refocusing precision of the modified SLIM algorithm in the condition of the same iteration

Table 4 Comparisons image Contrast of different algorithms
表4 不同算法图像对比度的对比

Noise	FFT	SLIM-FFT	Modified SLIM-FFT
0dB	1.45	2.46	2.66
-10dB	2.08	2.80	2.87
-20dB	2.30	2.81	2.86
-30dB	2.35	2.80	2.86
-40dB	2.36	2.81	2.85
No noise	2.36	2.80	2.85

number is better than the typical SLIM algorithm, as can be seen Fig. 7.

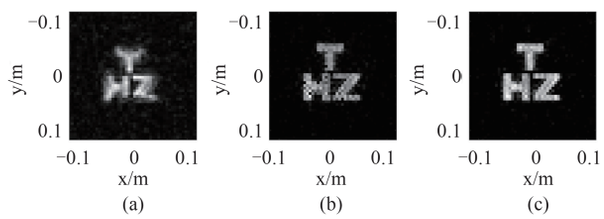

Fig. 7 (a) The original image generated by the FFT algorithm (b) The auto-focus image generated by the SLIM algorithm (iteration number = 2) (c) The auto-focus image generated by the modified SLIM algorithm (Th_dB = -20dB and iteration number = 2)
图7 (a)FFT算法初始图像 (b)SLIM算法自聚焦图像(迭代次数2) (c)改进SLIM算法自聚焦图像(Th_dB = -20dB,迭代次数2)

2.4 Number of iterations

The number of iterations required in the SLIM algorithm must be vital for computation efficiency. If the number of iterations is too large, the computational time may be too long, and if the number of iterations is too small, the quality of images may be poor.

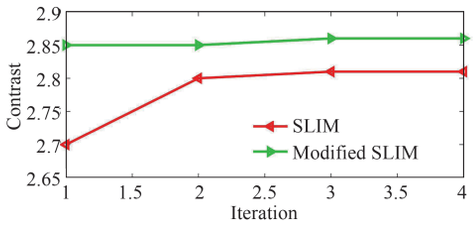

Fig. 10 The Contrast criteria of different iterations.
图10 不同迭代次数的对比度指标

The images of the SLIM algorithm and the modified SLIM algorithm without additive noise under different iterations are shown in Fig. 8 and Fig. 9; the curves of the contrast as a function of the iteration number are shown in Fig. 10. The values of the contrast display little change beyond the second iteration. And we note that, the modified SLIM algorithm reaches a stable contrast only after the first iteration, i. e. no iteration is actually needed at all, and at the meantime, the image contrast is higher for the same iteration number. The results verify that the modified SLIM algorithm can achieve reasonable image quality without any iteration process, thus further improves the computation efficiency.

3 Conclusions

An algorithm combining the PCA, FFT and modified SLIM auto-focus algorithms for millimeter-wave sparse planar array imaging is presented here. The distorted images generated by PCA and FFT are refocused by the modified SLIM algorithm to compensate the residual phase error introduced by the PCA. The simulations verify that the modified algorithm can achieve better images and higher computational efficiency, and compared to the original SLIM algorithm, no iteration is required. This proposed algorithm may find applications in through-the-wall radar imaging, ground penetrating imaging, nondestructive testing imaging, handheld millimeter-wave

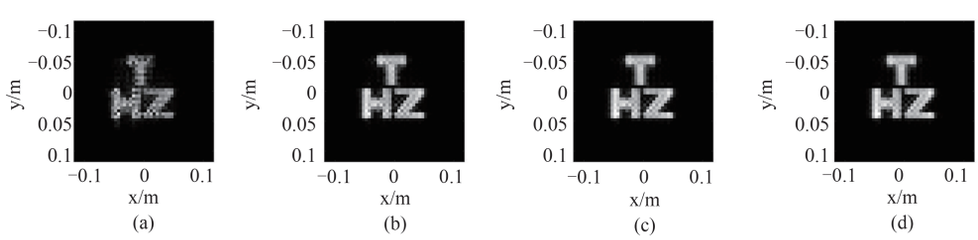

Fig. 8 Images under different iteration numbers of the SLIM algorithm. (a) 1 (b) 2 (c) 3 (d) 4
图8 SLIM算法不同迭代次数的图像 (a)1 (b)2 (c)3 (d)4

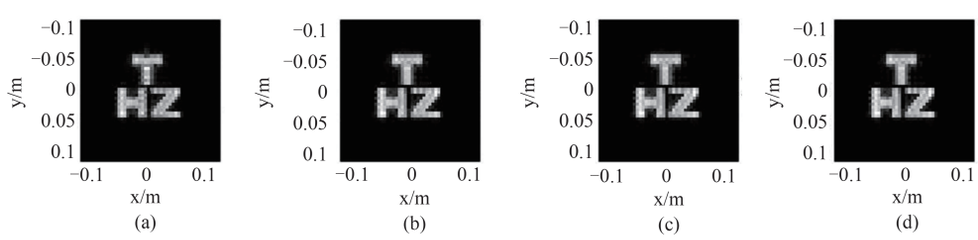

Fig. 9 Images under different iteration numbers of the modified SLIM algorithm (Th_dB = -20 dB). (a) 1 (b) 2 (c) 3 (d) 4
图9 改进SLIM算法不同迭代次数的图像(Th_dB = -20 dB) (a)1 (b)2 (c)3 (d)4

security inspection and remote sensing, etc.

References

[1] Meta A, Hoogeboom P. Development of signal processing algorithms for high resolution airborne millimeter wave FMCW SAR: IEEE International Radar Conference, 2005[C]. Arlington, USA, IEEE, 2005: 326-331.
[2] Nowok S, Kueppers S, Cetinkaya H, *et al*. Millimeter wave radar for high resolution 3D near field imaging for robotics and security scans: International Radar Symposium, 2017[C]. Prague, Czech Republic, IEEE, 2017: 1-10.
[3] Sheen D, McMakin D, Hall T. Three-dimensional millimeter-wave Imaging for concealed weapon detection[J]. *IEEE Transactions on Microwave Theory and Techniques*. 2001, **49**(9): 1581-1591.
[4] Sheen D, Hall T, Mcmakin D. Three-dimensional radar imaging techniques and systems for near-field applications[C]. Radar Sensor Technology XX. International Society for Optics and Photonics, 2016, **9829**: 1-12.
[5] Ahmed S, Schiessl A, Gumbmann F. Advanced microwave imaging [J]. *IEEE Microwave Magazine*, 2012, **13**(6): 26-43.
[6] Zhuge X D, Yarovoy A G. Three-dimensional near-field mimo array imaging using range migration techniques[J]. *IEEE Transactions on Image Processing*, 2012, **21**(6): 3026-3033.
[7] Moulder W F, Krieger J D, Majewski J J, *et al*. Development of a high-throughput microwave imaging system for concealed weapons detection: IEEE International Symposium on Phased Array System and Technology, 2016[C]. Waltham, MA, USA, IEEE, 2016: 1-6.
[8] Moulder F, Majewski J, Coldwell C, *et al*. Switched antenna array tile for real-time microwave imaging aperture: IEEE International Symposium on Antennas and Propagation & USNC/URSI National Radio Science Meeting, 2016[C]. Fajardo, Puerto Rico, IEEE, 2016: 1067-1068.
[9] Sheen D M, Hall T E, Severtsen R H. Standoff concealed weapon detection using a 350GHz radar imaging system [J]. *Proceeding of SPIE-The International Society for Optical Engineering*, 2010, **7670**(1): 115-118.
[10] Moulder W F, Krieger J D, Majewski J J, *et al*. Mobile tested for video-rate multistatic microwave imaging array: IEEE International Symposium on Antennas and Propagatio & USNC/URSI National Radio Science Meeting, 2019[C], Boston, MA, USA, IEEE, 2019: 3-4.
[11] Tan X, Roberts W, Li J, *et al*. Sparse learning via iterative minimization with application to mimo radar imaging[J]. *IEEE Transactions on Signal Processing*, 2011, **59**(3): 1088-1101.
[12] ZHAO Xia, WANG Xiong-Liang, WANG Zheng-Ming. Phase gradient autofocus algorithm for sar imagery based on contrast criteria[J]. *Remote Sensing Technology and Application*(赵侠, 汪雄良, 王正明. 基于最优对比度准则的*SAR*图像相位梯度自聚焦算法, **遥感技术与应用**), 2005, **20**(6): 606-610.